

Fuselage Drag Reduction Studies Using a Coupled Lattice Boltzmann and Navier-Stokes Methodology

Jee Woong Kim, Byung-Young Min, Lakshmi Sankar, Nandita Yeshala
School of Aerospace Engineering, Georgia Tech, Atlanta, GA, USA

T. Alan Egolf
Sikorsky Aircraft Corporation, Stratford, CT, USA

Abstract

Multi-scale modeling of synthetic jet devices with a coupled Lattice Boltzmann and Navier-Stokes methodology is employed to investigate the effect of active flow control (AFC) on fuselage drag reduction. The flow field in the vicinity of the synthetic jet devices was modeled using a Lattice Boltzmann equation (LBE) approach, while the external flow over the fuselage was modeled using a Reynolds-averaged Navier-Stokes (RANS) methodology. Benchmark problems are used to verify the coupled methodology. The method is next applied to the flow over an isolated fuselage of ROBIN-mod7 model. Computations with and without flow control also reported for flow field around the isolated fuselage. The computed results, in the absence of flow control, have been compared with the measured data for ROBIN-mod7 model and show good agreement up to the ramp area where turbulent separated flow effects require further studies. Results from the CFD simulation with AFC using LB/NS coupling methodology indicate in an estimated 27% drag reduction.

Nomenclature

R	= Reference rotor radius
f	= Excitation frequency, Hz
W	= Fuselage width (maximum)
A_{cs}	= Fuselage cross-sectional area (maximum)
q	= Freestream dynamic pressure $\equiv 1/2\rho_{\infty}U_{\infty}^2$
C_D	= Drag coefficient $\equiv \text{Drag} / (qA_{CS})$
F^+	= Reduced frequency $\equiv f W / U_{\infty}$
U_{∞}	= Freestream velocity
U_j	= Jet exit peak velocity

1. Introduction

A primary contributor to the drag of a helicopter is the pressure drag associated with separation from bluff geometries such as the fuselage, pylons, rotor hubs, and landing gear. The large separated region also affects flow over near-by aerodynamic surfaces (such as the rotors and stabilizers) increasing the interference drag. It is highly desirable to reduce the vehicle drag by delaying or suppressing of the flow separation.

Several computational and experimental flow control studies [1,2] have been done to over the years that employ active flow control for fuselage drag reduction. Early active flow control (AFC) studies used steady blowing or suction devices that are located in the vicinity of the separation line. Although these methods are effective in drag reduction there are some deficiencies due to weight increases, mechanical complexity, and additional power required. Zero mass flow rate jets, known as synthetic jets or pulsed jets have also been studied [3,4]. A synthetic jet utilizes periodic excitation of mass flow which is achieved

with the use of relatively small piezoelectric plates or electromechanical piston arrangements in cavities. Fuselage drag reduction using synthetic jet devices is the subject matter of the present numerical study.

The flow field around fuselage that employs active flow control devices is a multi-scale phenomenon. The flow in the vicinity of the synthetic jet devices is dominated by small length and time scale incompressible phenomena. It is computationally inefficient to use compressible flow solvers in incompressible regions. A Lattice Boltzmann equation (LBE) solver is suitable for economically resolving these features. The outer flow over the fuselage, the boundary layer, and the separated flow are dominated by larger time and spatial scale events. These events are best modeled using a Reynolds-averaged Navier-Stokes (RANS) solver. Since the flow in the vicinity of the AFC devices influence the outer flow field and vice versa, these two models should be temporally and spatially coupled, in a manner that conserves mass, momentum, and energy at the interfaces.

An LBE solver has been developed by the present authors [5,6] and has subsequently coupled with an existing Navier-Stokes (NS) solver [7,8]. Validations of each solver and the coupled methodology have been done for several benchmark cases. The present study discusses the application of this multi-scale approach (coupled LBE and RANS methodology) for the reduction of fuselage drag using AFC. Computations are performed for flowfield around the isolated fuselage of ROBIN-mod7 model [9] with and without active flow control. The computed results are compared and correlated with results from the measured data for ROBIN-mod7 model.

2. Numerical Methods

A 3D Reynolds-Averaged compressible Navier-Stokes solver called GENCAS (Generic Numerical Compressible Airflow Solver), developed by Min [7,8] is used in this study to model the outer flow field. This solver may be used to study viscous flow phenomena on 2D or 3D structured multi-block grids. Roe's FDS and AUSMPW+ upwind schemes are available for computing the inviscid flux. First or second order implicit LUSGS with Newton sub-iteration, and a 2nd/4th order explicit Runge-Kutta schemes are available as user-selected options for marching in time. If higher order accuracy is desired, 3rd order upwind schemes, 5th order weighted essentially non-oscillatory (WENO5) methodologies or a 7th order upwind (WENO7) cell interface reconstruction methods may be selected. Numerous

turbulence models include one equation Spalart-Allmaras (SA) and SA-DES models, and two equation Wilcox's $\kappa-\omega$, standard $\kappa-\epsilon$, Menter's $\kappa-\omega/\kappa-\epsilon$ BSL, Menter's $\kappa-\omega$ SST, KES [10,11], and a hybrid RANS-subgrid kinetic energy simulation (HRKES) [12,13] are available [Ref.] models. For a detailed description of the numerical formulation of GENCAS, the reader is referred to the papers written by Min et al. [7,8]. In the present study, a Roe scheme with a 3rd order MUSCL reconstruction is used for flux calculations. First order implicit LUSGS with Newton sub-iteration is used for marching in time. Spalart-Allmaras (SA) is used as a turbulence model.

The LBE method simulates flowfield by tracking the evolution of particle distributions instead of tracking particles as in the case of Lattice gas automata (LGA). It also differs from the traditional CFD methods in that it does not directly solve for macroscopic variables which appear in the Navier-Stokes equations. LBE recovers the Navier-Stokes equation using the Chapman-Enskog expansion [14, 15]. Solving LBE has the following advantages over Navier-Stokes equations. First, the convection operator in LBE is linear which is much faster and easier to compute than the non-linear advection term in Navier-Stokes equations. Secondly, the Poisson equation, which is difficult to solve, is not solved in LBE since the macroscopic properties of the flow field are not directly calculated. Finally, the macroscopic properties of the flow are obtained by simple arithmetic integration of microscopic properties in LBE and are therefore easier to implement.

The LBE method and its coupling with NS solver have been previously validated. Details of the LBE solver, the coupling approach, validation studies using benchmark test cases, and application to 2-D drag reduction are described in Reference 5 and 6.

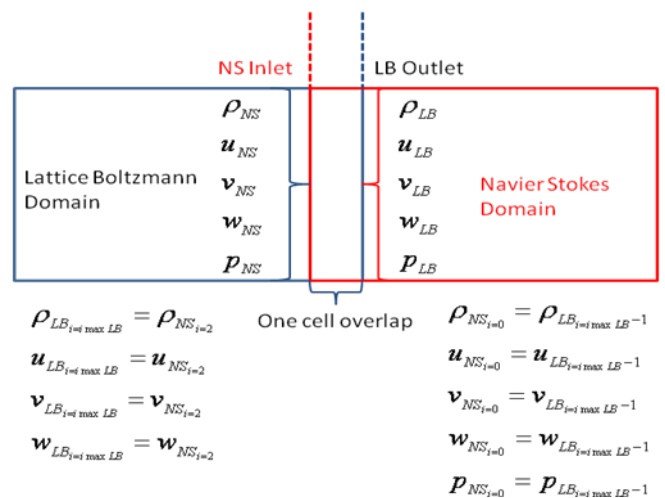


Figure 1. Information exchange between LB and NS solvers.

2-1. Boundary condition formulation for coupling the LBE and RANS methodologies

The present coupling method uses a one cell overlap between the LB and RANS (node-centered) solvers where the information is exchanged between the two solvers. Figure 1 summarizes this formulation. In this figure, “ i ” represents the i^{th} node in each of the domains and $i_{\text{max,lb}}$ represents the maximum i^{th} node in the LB domain. $I=0$ represents the ghost cell location in the NS solver.

At the interface, the LB microscopic values are converted into macroscopic density, velocities and pressure. If a node-to-node matching grid system is used, these macroscopic values are passed to the NS solver at the corresponding nodes. This information is used as a “ghost cell” data when formulating the characteristic inflow/outflow type boundary condition at the inlet, $i = 1$.

The microscopic density and velocity values are obtained by converting the macroscopic values from the Navier-Stokes solver. These values are used as the boundary condition at the LB interface. This information exchange between the Navier-Stokes and LBE solvers is performed at every time step.

The extension of the coupled methodology for curvilinear surfaces (Figure 2) is performed by using linear interpolation of the flow field quantities at the curved surface. This interpolation is sufficient for the present studies since the grid spacing in the region of use is very small and the gradients within one cell are not large. Although the boundary condition is locally first-order accurate, the solution is still globally second-order accurate due to the spatially second-order accurate solvers used. This is similar to the method used by well-established solvers such as OVERFLOW, where a local first-order accurate boundary condition is used in globally second-order accurate solver.

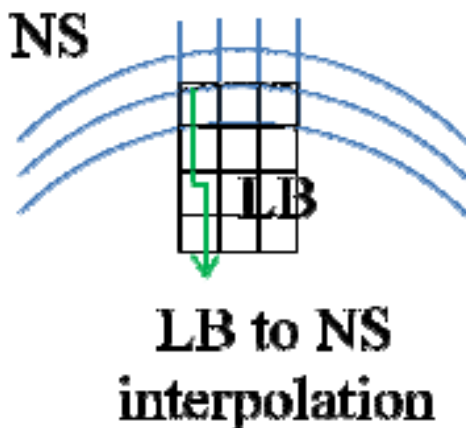


Figure 2. Coupled methodology for curved surfaces.

Note that the LBE solver does not account for the effects of turbulent eddies. The flow in the vicinity of the synthetic jet cavity is incompressible. The LBE domain extends only into the laminar sublayer of the NS flow. However, turbulence modeling has been used in the outer flow over the fuselage.

3. Results and Discussions

Prior to the use of the coupled LBE + RANS solvers, these two solvers have been independently tested. These validation studies are briefly described below.

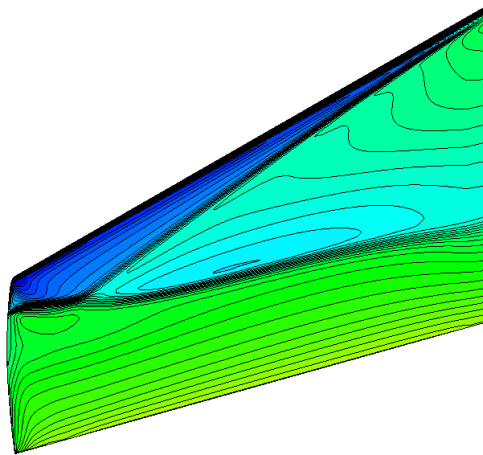
3-1. Validation of Navier-Stokes solver

A half-wing model ONERA-M6 reported in AGARD test data base [16] is a classical three dimensional validation case suitable for CFD code assessment. The model is a swept back wing with an aspect ratio of 3.8 and taper ratio of 0.562. The mean aerodynamic chord length is 0.64607m and the semi-span is 1.1963m. The wing has been tested in the ONERA S2MA wind tunnel at transonic Mach numbers and the surface pressure distributions were obtained at several span sections. The selected case was tested at Mach number of 0.84 with angle of attack of 3.06 degrees. The Reynolds number based on chord length is 11.72 million. The λ shape shock wave on the upper surface was well captured with both S-A and KES turbulence models (Figure 3). The C_p distributions showed in Fig. 4 at several span sections show good correlation with test data for both the S-A and KES turbulence models. The leading edge suction and following shock wave locations were well predicted.

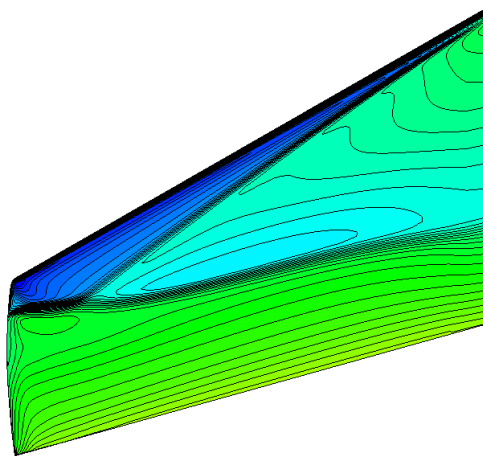
3-2. Active flow control using the coupled Lattice Boltzmann-Navier-Stokes methodology for flow past a cylinder

Active flow control has been applied to the three-dimensional flow past a cylinder. In order to examine the effect of the active flow control, computations with and without AFC are performed for a Reynolds number of 75500, based on the cylinder diameter of 0.0632m. The time-averaged pressure data from the three-dimensional simulations are in considerably better agreement with test data compared to the two-dimensional case, as shown in the C_p comparison in Figure 5. The drag coefficient calculated in the three-dimensional simulation, 0.9468, is within 1% of the experimental value of 0.95. It is thus concluded that the simulations agree well with experiment forming a baseline condition against which AFC studies may be compared.

The configuration for the 3D cylinder with AFC is shown in Figure 6. The synthetic jets are activated over specified spanwise locations as shown in Figure 6. Spanwise adjacent synthetic jets are set to be 180 degrees out of phase with each other in order to break the coherence of the flow. At each spanwise location, two synthetic jet slots are placed at approximately 110° aft of the front stagnation point of the cylinder. Figure 7 shows the time-averaged C_p distribution on the surface of the cylinder. The phase-lagged synthetic jets show a suction peak in the pressure at the location of the jets and an improved pressure recovery is observed behind the cylinder. The drag obtained from AFC is 0.87 which is 8.5% less than that obtained from the baseline. Analysis of the flowfield was performed in order to observe the synthetic jet action. High pockets of velocity are observed to emerge alternatively from the spanwise adjacent jets as seen in the instantaneous Mach number contours in Figure 8. The coherence of the vortex structures in the separated flow region is broken up due to the lag in the suction and the blowing phase between the jets.



(a) S-A model



(b) KES model

Figure 3. Surface pressure contour.

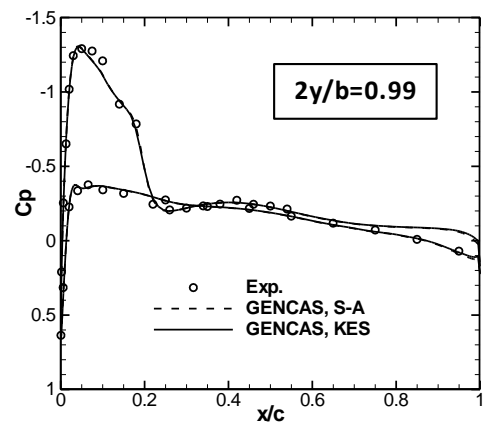
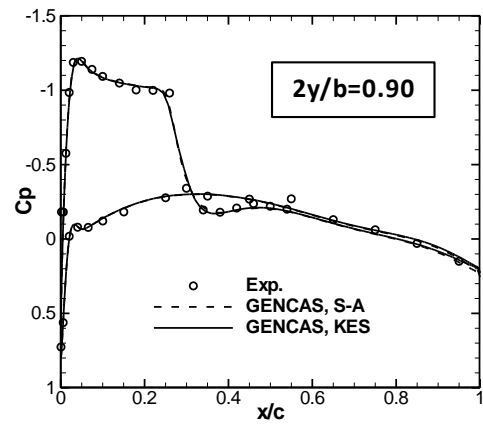
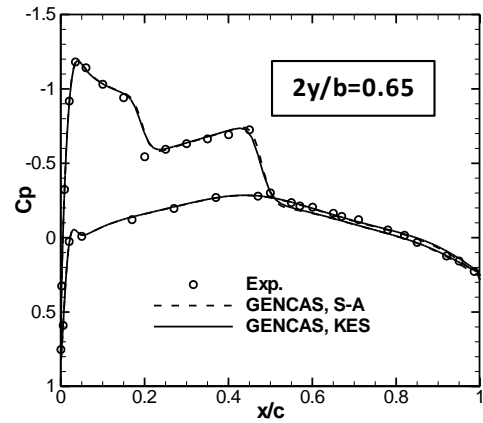
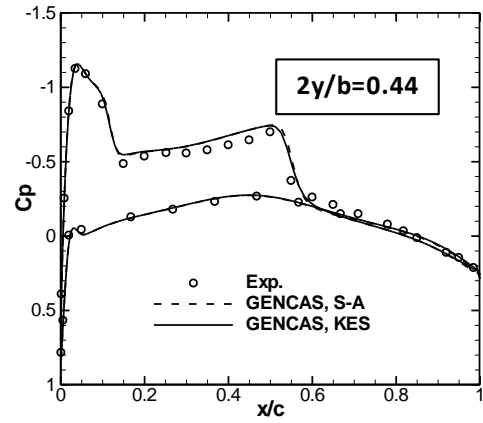


Figure 4. Surface C_p distributions.

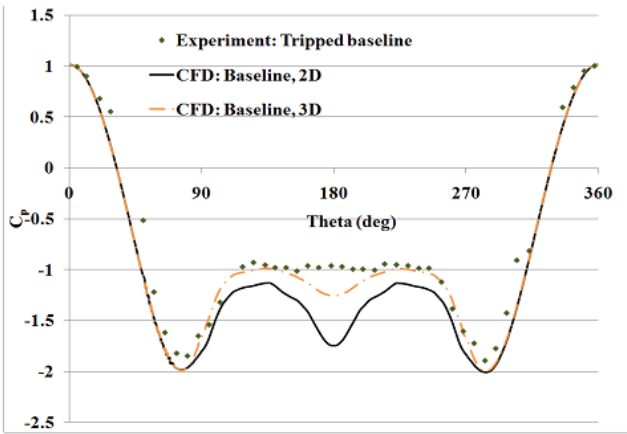


Figure 5. Comparison of C_p between experiment and two-dimensional as well as three-dimensional simulations.

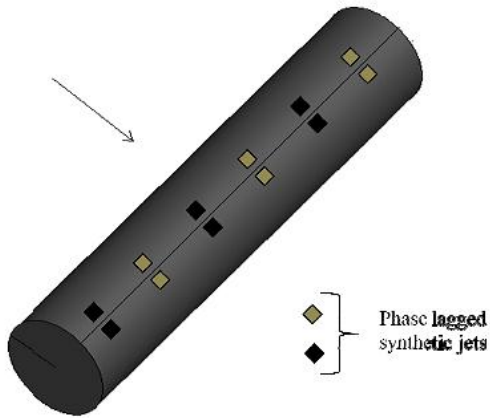


Figure 6. Configuration of 3D cylinder with active flow control slots.

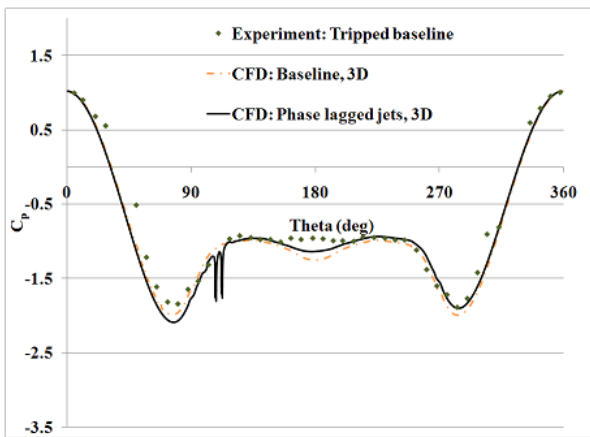
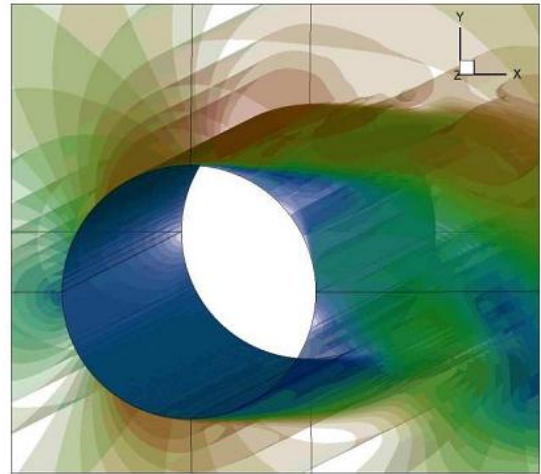
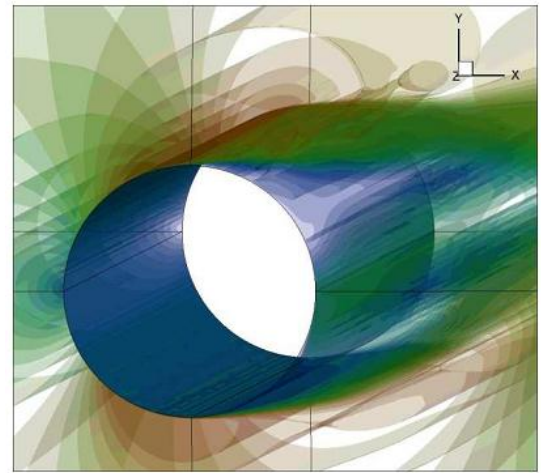


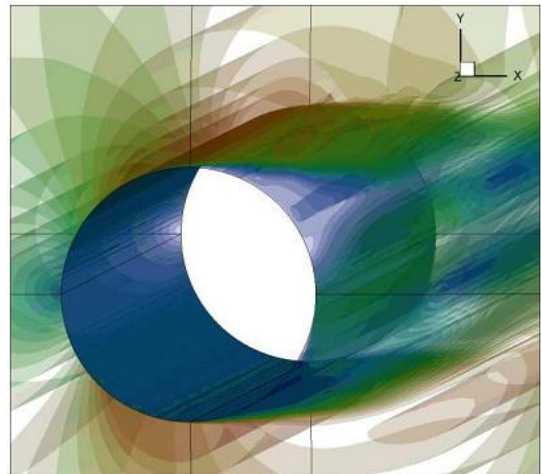
Figure 7. Comparison of time-averaged C_p distribution on the surface of the 3D cylinder.



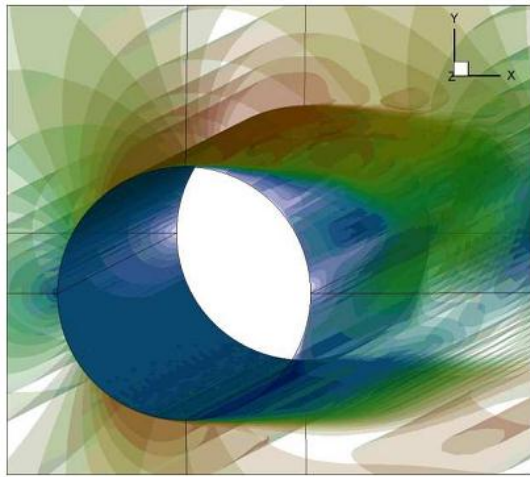
(a)



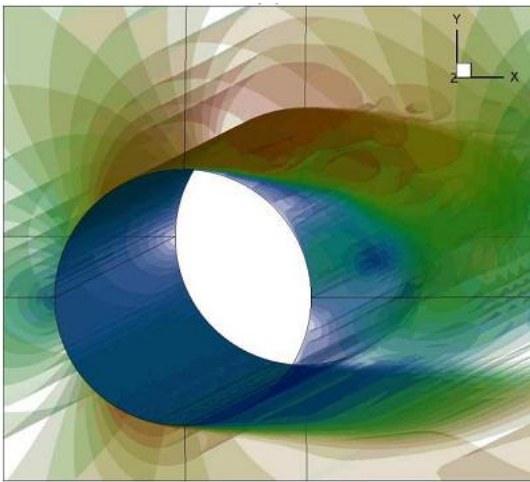
(b)



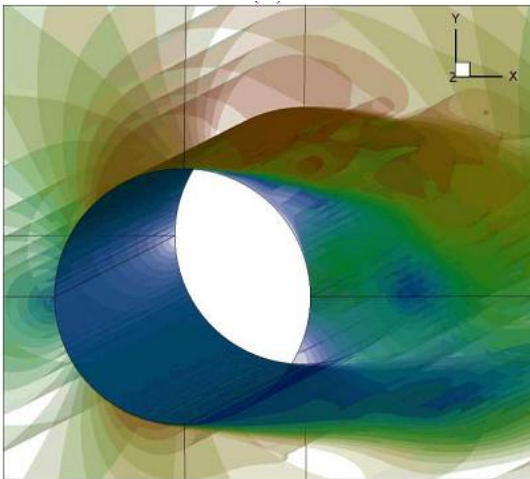
(c)



(d)



(e)



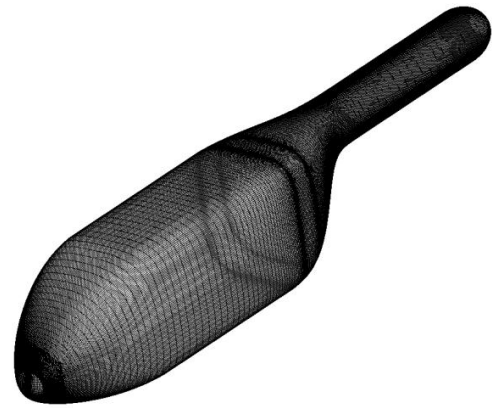
(f)

Figure 8. Instantaneous Mach number contours around the 3D cylinder with phase-lagged synthetic jets.

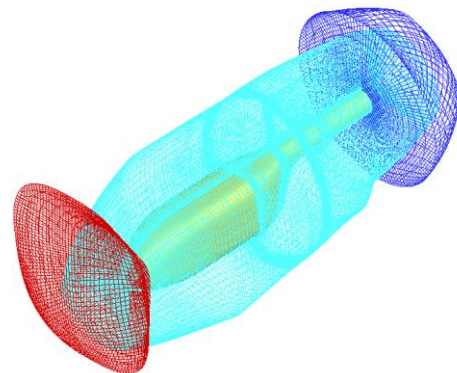
3-3. Active flow control for isolated fuselage of ROBIN-mod7 model

3-3-1. Baseline Case

Computations have been performed for a baseline ROBIN-mod7 model without flow control. Navier-Stokes equations are solved implicitly using LUSGS scheme with a 3rd order MUSCL scheme for the inviscid flux terms. Spalart Allmaras turbulence model was used. The wind tunnel tests were conducted at NASA Langley Research Center. The fuselage model is 0.7172m in length. An isolated fuselage was tested. Table 1 shows the test conditions for the baseline case. Freestream velocity is approximately 34m/s, corresponding to a Mach number of 0.1 and a Reynolds number, based on the length of the fuselage is 1.6 Million. Overset grids are used to compute flowfield around the ROBIN-mod7 model. Figure 9 shows the overset grid system used in this study.



(a) Surface mesh



(b) Overset grids

Figure 9. Grid system for the ROBIN-mod7 fuselage.

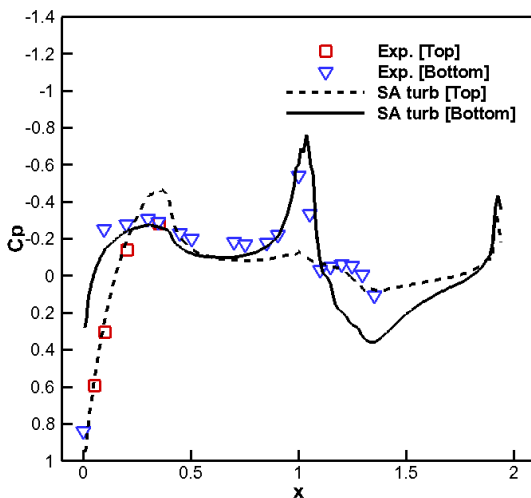
Table 1. Test conditions for baseline case.

Freestream Mach number	0.1
Reynolds number	1.6×10^6
Angle of attack	0 deg.

Table 2. Grid system.

Grid	Number of mesh points
Nose cap	54 x 37 x 37
Fuselage	191 x 65 x 49
Tail cap	49 x 33 x 33
Background	98 x 81 x 81

Table 2 gives details of the number of grid points within each of the overset meshes. The centerline C_p values are compared to the experimental data in Fig. 10. Present Computations shows good agreement with experiment near fuselage nose. There are significant differences between the simulations and the test data near the ramp region where flow separation occurs. Improvement of the pressure correlation may be obtained using additional embedded or overset grids in this region. A summary of C_D values and a break-down of the viscous and pressure contributions are given in Table 3. Because the present simulations overestimate the pressure recovery in the ramp region, the computed pressure drag is lower than the actual pressure drag. The skin friction drag, with the fully turbulent flow, is higher. The overall drag coefficient matches well with test data, but this agreement is spurious. Therefore, in present study, we only focus on the “delta” reductions of the drag coefficient attributable to active flow control, rather than the absolute values of C_D .

**Figure 10. Comparison of the centerline surface C_p values (baseline case).****Table 3. Summary of the baseline drag comparison.**

	C_{Dvisc}	C_{Dpress}	C_D
Experiment			0.145
SA model	0.064	0.081	0.145

3-3-2. Active flow control studies

Numerical results for the active flow control are next presented. In addition to the coupled LB-NS simulations, NS simulations without LB modeling of the devices have also been performed. These are done by specifying the jet properties (e.g. momentum coefficient of the jet and the jet angle) at the fuselage surface. The jet inclination angle is specified and based on the local surface tangent, normal to the slot span. 90 degree of jet inclination angle means that it is normal to the local surface and zero is tangent to the local surface and normal to the slot local spanwise tangent. In this study, 4 flow control synthetic jet slots are employed. These are located near the flow separation region and constructed by finding the intersection of a plane that originated at a constant longitudinal location (x/R). This plane is rotated 23 degree about an axis formed by the intersection of the x/R location and $z/R=0$ planes [9]. Figure 11 shows the side and rear view of slot locations. The slots are located at $x/R=1.155$ and a slot width of 0.001 (h/R) is used. As discussed earlier, the flowfield inside the cavity is modeled using LBE while the flowfield around fuselage is solved by NS solver. The jet velocity ratio, U_j / U_∞ , is 0.2. A jet inclination angle of 15 degree is used for the RANS-alone simulations without the LBE model of the device. The velocity of synthetic jet is defined as:

$$U_j = U_j \sin(2\pi ft + \phi)$$

where f is the frequency and ϕ the phase. Reduced frequency of $F^+=0.33$ and same phase for all slots are used.

The results from the CFD simulations are presented in Fig. 12 and Table 4. The RANS-alone calculations, where the synthetic jet was modeled only through boundary conditions in NS solver, indicate a drag reduction of 30% relative to the baseline. The fully coupled LBE/NS analysis indicated a drag reduction of 27.5% compared to baseline. From Fig. 12 it is seen that there is phase delay of the C_D as a function of time between two AFC simulations. However, the amplitudes of fluctuation are nearly the same. The NS simulation without LB modeling shows a higher drag reduction presumably because the entire slot area has same jet velocity. The LBE solver, because it captures the viscous flow inside the devices, has a turbulent jet profile that goes to zero at the solid boundaries of the slot.

Figure 13 shows a comparison of surface pressure distributions near the ramp region. The flow control case shows a greater pressure recovery in the ramp region compared to the baseline case, causing a reduction in pressure drag. Figure 14 shows Mach number contours with streamlines near synthetic jet. Flow separation occurs between $x/R=1.09$ and $x/R=1.1$. Figure 15 shows comparison of the corresponding vorticity contours at $x/R=1.2$. The baseline simulations without AFC indicate the presence of stronger vortex structures relative to the active flow control case. It is also found that vortices are diffused as a result of flow control.

Table 4. Summary of the drag comparison.

	C_D	% reduction
Baseline	0.145	
AFC with NS only	0.100	30.7
AFC with LB/NS coupling	0.105	27.5

4. Summary and Recommendations

A coupled Lattice Boltzmann and Navier-Stokes methodology has been developed and employed to investigate the effect of active flow control (AFC) on drag reduction. The Navier-Stokes solver, and the coupled Lattice Boltzmann and Navier-Stokes methodology have been validated for benchmark cases prior to their application in the present work. Studies for fuselage drag reduction using AFC have been presented for the ROBIN-mod7 fuselage. For the baseline case without AFC, reasonable predictions of C_p and total drag coefficient were obtained except in the ramp region where unsteady separated flow is present. Additional work is needed to better capture the pressure recovery in the ramp region. Synthetic jet simulations have been done using the RANS solver alone, and with a combined LB/RANS approach. These studies show a 27.5% reduction of drag coefficient. Further studies of the flow field, with embedded finer grids in the separated flow region, is necessary to better understand the physical processes responsible for the drag reduction.

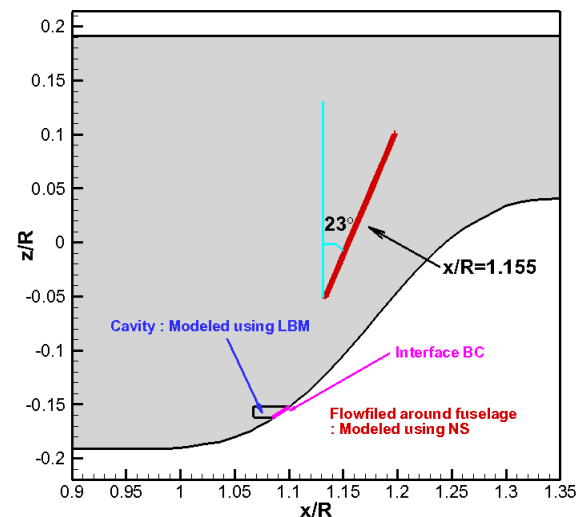
Acknowledgments

This project was funded by the U. S. Army under the Vertical Lift Research Center of Excellence (VLRCE) program managed by the National Rotorcraft Technology Center, Aviation and Missile Research, Development and Engineering Center under Cooperative Agreement W911W6-06-2-0004 between Georgia Institute of Technology and the U. S. Army Aviation Applied Technology Directorate. Dr. Michael Rutkowski is the technical monitor. The authors would like to acknowledge that this research and

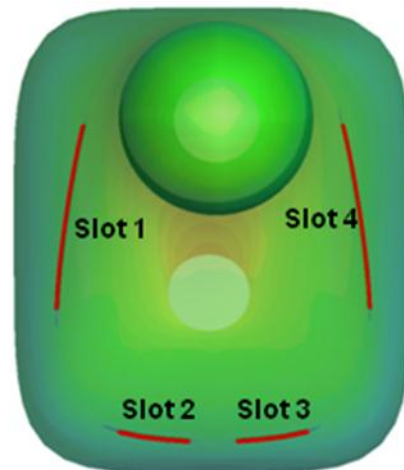
development was accomplished with the support and guidance of the NRTC. The views and conclusions contained in this document are those of the authors and should not be interpreted as representing the official policies, either expressed or implied, of the Aviation and Missile Research, Development and Engineering Center or the U.S. Government.

REFERENCES

- [1] Martin, P., Tung, C., Hassan, A., Cerchie, D., and Roth, J., "Active Flow Control Measurements and CFD on a Transport Helicopter Fuselage," American Helicopter Society 61st Annual Forum, Grapevine, TX, 2005.
- [2] Ben-Hamou, E., Arad, E., and Seifert, A., "Generic Transport Aft-Body Drag Reduction using Active Flow Control," AIAA Paper 2004-2509, 2004.
- [3] Amitay, M., Smith, B. L., and Glezer, A., "Aerodynamic flow control using synthetic jet technology," 36th AIAA Aerospace Sciences Meeting 98-0208, Reno, Nevada, 1998.



(a) Side view



(a) Rear view

Figure 11. Slot locations.

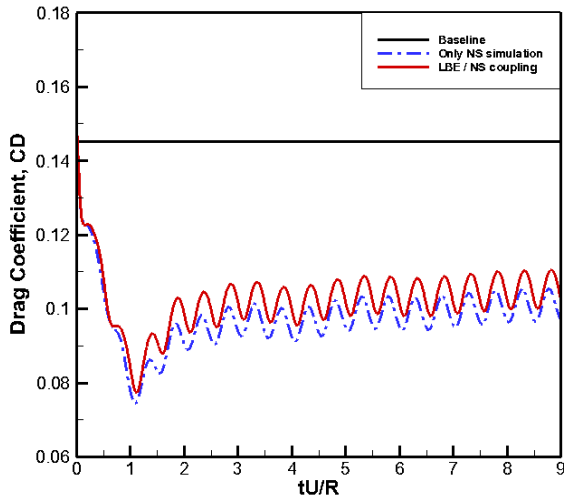
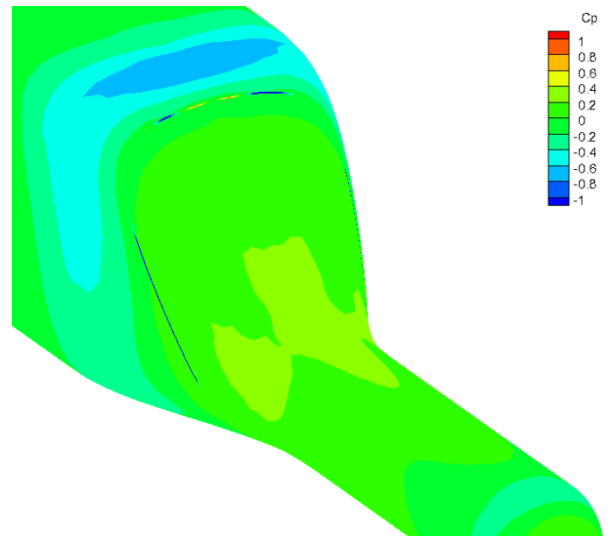
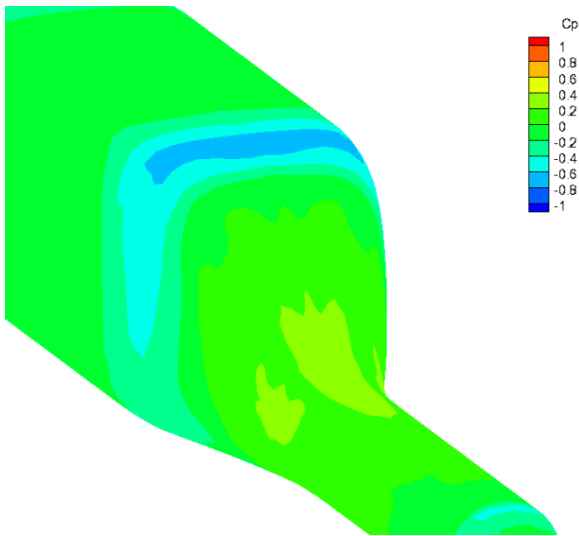


Figure 12. Time history of drag coefficient for flow control.

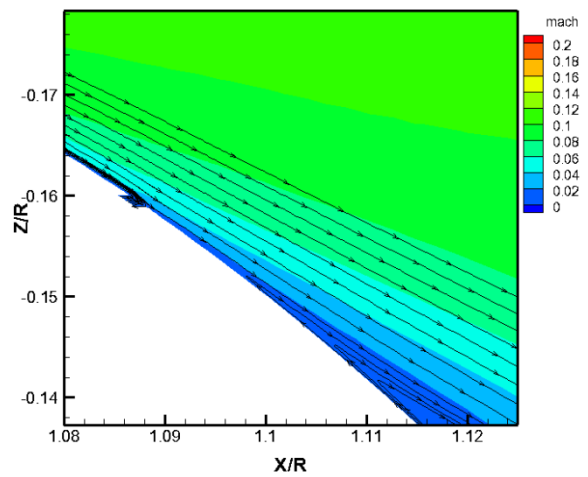


(c) LBE/ NS coupling (Blowing part of cycle)

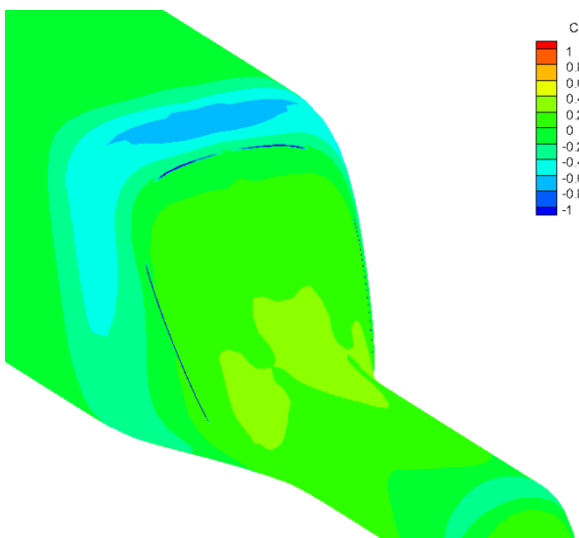
Figure 13. Comparison of surface pressure distributions.



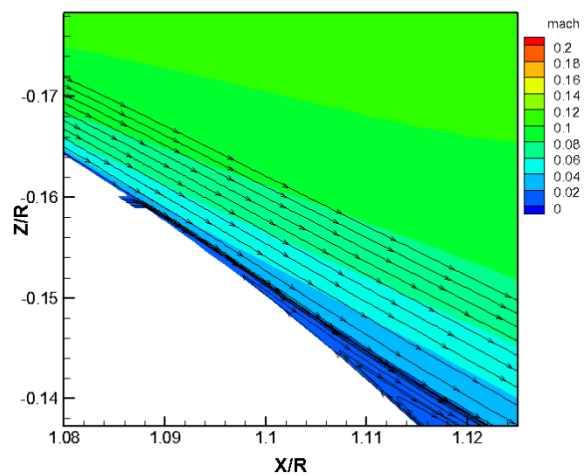
(a) Baseline



(a) LBE/ NS coupling (Suction part of cycle)

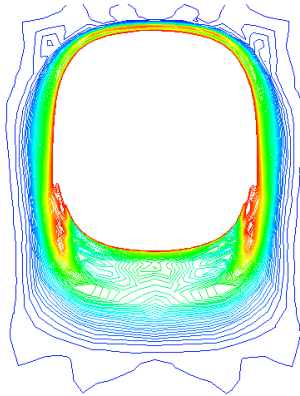


(b) LBE/ NS coupling (Suction part of cycle)

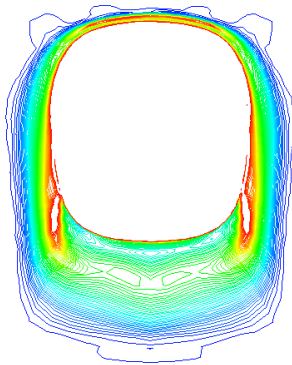


(b) LBE/ NS coupling (Blowing part of cycle)

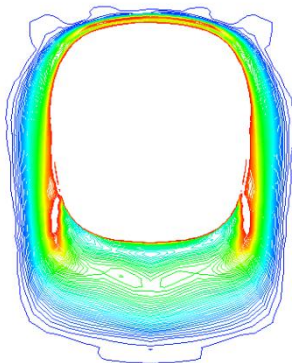
Figure 14. Mach number contour with stream line.

Vorticity contour at $X/R = 1.2$ 

(a) Baseline without AFC

Vorticity contour at $X/R=1.2$ 

(b) LBE/ NS coupling (Suction part of cycle)

Vorticity contour at $X/R=1.2$ 

(b) LBE/ NS coupling (Blowing part of cycle)

Figure 15. Comparison of vorticity contour at $x/R=1.2$.

- [4] Ben-Hamou, E., Arad, E., and Seifert, A., "Generic Transport Aft-Body Drag Reduction using Active Flow Control," AIAA Paper 2006-2509, 2nd AIAA Flow Control Conference, Portland, OR, 28 June – 1 July 2004.
- [5] Yeshala, N., "A Coupled Lattice Boltzmann-Navier-Stokes Methodology for Drag Reduction," Ph. D Dissertation, Georgia Institute of Technology, Atlanta, GA, November 2010.
- [6] Yeshala, N., and Sankar, L. N., "Three-Dimensional Active Flow Control Drag Reduction Studies Over a Bluff Body Using a Coupled Lattice Boltzmann and Navier-Stokes Methodology," 49th AIAA Aerospace Sciences Meeting, Orlando, Florida, January 2011.
- [7] Min, B. Y. and Sankar, L. N., "Enhancements to a Hybrid Navier-Stokes/Free Wake Method for Improved Prediction of Blade-Vortex-Interaction Phenomena," AIAA 2009-3860, 27th AIAA Applied Aerodynamics Conference, San Antonio, Texas, June 22-25, 2009.
- [8] Min, B. Y., Lee, W., Englar, R. and Sankar, L. N., "Numerical Investigation of Circulation Control Airfoils," Journal of Aircraft, vol. 46, No. 4, pp. 1403-1410, 2009.
- [9] Norman W. Schaeffler, Brian G. Allan, Caroline Lienard and Arnaud Le Pape, "Progress Towards Fuselage Drag Reduction via Active Flow Control: A Combined CFD and Experimental Effort," 36th European Rotorcraft Forum, Paris, France, Sep. 7-9, 2010.
- [10] Fang, Y., and Menon, S., "A Two-Equation Subgrid Model for Large-Eddy Simulation of High Reynolds Number Flows," AIAA paper 2006-116, 44th AIAA Aerospace Sciences Meeting and Exhibit, Reno, Nevada, 9-12 January, 2006.
- [11] Fang, Y., and Menon, S., "Kinetic Eddy Simulation of Static and Dynamic Stall," AIAA 2006-3847, 24th Applied Aerodynamics Conference, San Francisco, California, 5-8 June, 2006.
- [12] Zaki, M., Menon, S., and Sankar, L. N., "A Hybrid RANS/KES Model for External and Internal Flow Applications," AIAA 2008-5216, 44th AIAA/ASME/SAE/ASEE Joint Propulsion Conference and Exhibit, Hartford, CT, 21-23 July, 2008.
- [13] Zaki, M., "Physics Based Modeling of Axial Compressor," Ph. D. Dissertation, School of Aerospace Engineering, Georgia Institute of Technology, Atlanta, GA, 2009.
- [14] Qian Y., d'Humières D., and Lallemand P., "Lattice BGK Models for Navier-Stokes Equation," Europhysica Letters, vol. 17(6), pp. 479-484, 1992.

- [15]Chen H., Chen S., and Matthaeus W. H.,
“Recovery of the Navier-Stokes equations using a
lattice-gas Boltzmann method,” Physical Review
A, vol. 45, Issue 8, pp. 5339-5342, 1992.
- [16]Schmitt, V. and Charpin, F., "Pressure
Distributions on the ONERA-M6-Wing at
Transonic Mach Numbers," Experimental Data
Base for Computer Program Assessment. Report
of the Fluid Dynamics Panel Working Group 04,
AGARD AR 138, May 1979.